Formation of copper oxide surface structures via pulse injection of air onto Cu(111) surfaces

C. Pérez León,[1,*] C. Sürgers,[1] and H. v. Löhneysen[1,2]

[1]*Karlsruhe Institute of Technology (KIT), Physikalisches Institut and DFG-Center for Functional Nanostructures (CFN), P. O. Box 6980, D-76049 Karlsruhe, Germany*

[2]*Karlsruhe Institute of Technology (KIT), Institut für Festkörperphysik, P. O. Box 3640, D-76021 Karlsruhe, Germany*

(Received 27 May 2011; revised manuscript received 23 December 2011; published 20 January 2012)

We have investigated the Cu(111) surface after controlled injection of air by Auger electron spectroscopy (AES) and scanning tunneling microscopy (STM). During deposition, the temperature of the copper substrate was kept at room or elevated temperature. AES spectra show that mainly oxygen is adsorbed on the copper surface. STM images display the initial stages of oxidation of Cu(111), which are governed by the restructuring of the surface where Cu atoms from the step edges and terraces are incorporated into the growing surface oxide. The nucleation and growth of the oxide are strongly influenced by the substrate temperature during air injection as well as by the oxygen coverage. Depending on the coverage, different kinds of oxide or oxide-precursor islands are observed. The surface oxides produced at higher temperature exhibit ordered structures, which are ascribed to a strained $Cu_2O(111)$ lattice that coincides with the Cu(111) substrate.

DOI: 10.1103/PhysRevB.85.035434 PACS number(s): 81.16.Pr, 68.37.Ef, 68.35.B−

I. INTRODUCTION

The deposition of organic molecules on metal substrates has been extensively studied in recent years because of the increasing interest in functional materials and molecular electronics. Scanning tunneling microscopy (STM), in particular when operated under ultrahigh vacuum (UHV) conditions, has become the most widely used technique to investigate such systems since it provides high spatial resolution of the topographic and electronic structure of the molecules. Obtaining high-quality STM images of individual molecules requires a reliable sample preparation method. The most common method for depositing organic molecules under UHV conditions is thermal evaporation or sublimation. This method, however, can not be applied to reactive molecules nor to large molecules because in many cases they decompose before sublimation. Thus, other methods have to be used to deposit large molecules such as DNA, carbon nanotubes, polymers, or macrocycles in UHV. A very promising deposition method is pulse injection,[1] where a solution of the molecules under investigation is injected into the UHV chamber using a high-speed pulse valve. When the solvent enters the chamber, it vaporizes quickly, ideally leaving only the molecules under investigation on the substrate's surface. Compared with other solution-based deposition methods, this approach has the advantage that the sample is prepared *in situ*. However, prior to deposition, when the solution is introduced into the inlet of the pulse valve, it is for a short time exposed to ambient atmosphere. It is thus difficult to avoid that a small amount of air is dissolved into the solution, or that a thin cushion of air remains between the solution and the valve, entering the chamber before the solution does, thus contaminating the substrate. Therefore, a study of the potential effects of such impurities on the substrate surface is of considerable interest. Furthermore, the chemical reaction with air and, in particular, with gaseous oxygen, plays a key role in a broad range of applications, especially in catalysis and corrosion processes. Therefore, many groups have studied the oxidation of copper surfaces.[2–18] In the bulk, cubic Cu_2O and monoclinic CuO are the only binary copper-oxygen compounds.[19] Under vacuum conditions, mainly Cu_2O grows on the copper surface.[20,21]

In this paper, we present the results of our investigations by Auger electron spectroscopy (AES) and STM of clean Cu(111) surfaces after injection of air for different coverages when the substrate is kept at room and at elevated temperatures. Our observations will be discussed in comparison with previous works.

II. EXPERIMENT

In order to carry out the pulse-injection deposition, a specially designed molecular deposition chamber was used (details can be found in Ref. 22). The Cu(111) substrate (MaTecK GmbH) was prepared by several cycles of 1–3 keV Ar^+ sputtering and subsequent heating up to 550 °C. The surface has been imaged by STM (STM1, Omicron NanoTechnology GmbH). The cleanliness of the surface was confirmed by AES using a cylindrical-mirror analyzer and an excitation energy $E_e = 3$ keV.

The base pressure in the deposition chamber was lower than 2×10^{-9} mbar. For the injection of air, the sample was placed in a horizontal position 10 cm below the nozzle of the pulse valve. The valve was opened for a short time of $\approx$10 ms, once or several times, in intervals of several minutes, which is the time needed for recovering the base pressure. In general, one pulse was sufficient for air deposition, although the procedure was repeated when the pressure did not reach the desired coverage. During the opening of the valve, the pressure increased to 1×10^{-7}–5×10^{-6} mbar and recovered within a few minutes, resulting in an brief exposure to air of few seconds at the higher pressure. After completion of the deposition, the sample was transferred to the analysis chamber where the base pressure was lower than 1×10^{-10} mbar. The sample was subsequently imaged by STM using W tips, which were prepared by electrochemical etching and further cleaned in UHV by heating and Ar^+ ion sputtering. All STM images were obtained at room temperature (RT) in the constant-current mode. The majority of the presented STM images were filtered using the fast-Fourier-transform procedure and the drift, and

minor distortions in the raw images were reduced by slightly changing the piezo voltage-strain calibration to yield the sixfold symmetry of the Cu(111) surface.

III. RESULTS

A. Clean Cu(111) surface

Figure 1 shows STM images of the clean Cu(111) surface. The terraces have widths of several tens of nanometers and smooth step edges. Steps separating the terraces are usually monoatomic. Defects corresponding to small islands of vacancies are observed on the surface. Figure 1(b) shows an image obtained with atomic resolution where the hexagonal structure of the fcc (111) surface is resolved. The arrows indicate the three equivalent ⟨110⟩ directions in the (111) plane.

B. Auger spectroscopy after injection of air

Prior to STM, the copper surface was investigated with AES. As expected, a direct correlation between the increase of the pressure of the deposition chamber after opening of the valve and the coverage on the sample was found: the higher the rise of pressure, the higher the coverage. We also observed that the longer the opening time of the valve, the higher the coverage was. In general, only one pulse was used.

Figure 2 shows Auger spectra of the Cu(111) surface before and after pulse injection of air, resulting in a one monolayer coverage as inferred from the STM image when the substrate was kept at ∼200 °C (see Sec. III D). Here and in various other experiments, aside from the oxygen peak, a weak carbon peak is observed, which is attributed to CO_2 molecules or to other carbon-containing impurities that are dissolved in air. Less likely is the possibility that residues of

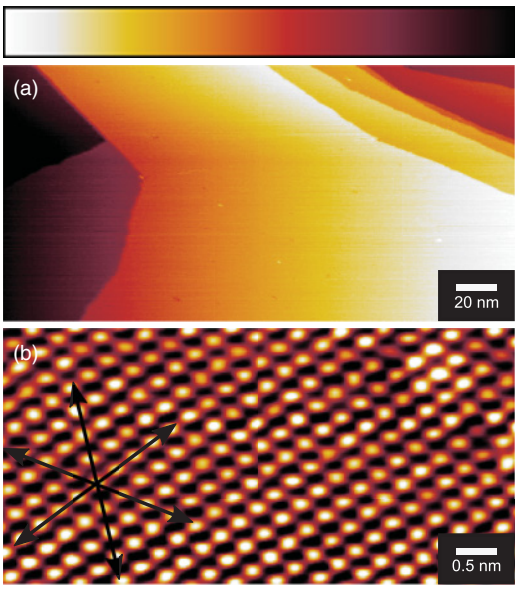

FIG. 1. (Color online) STM images of the clean Cu(111) surface at RT. (a) Step edges: image size 200 × 100 nm^2. (b) Atomic resolution: 5 × 2.5 nm^2, height scale 0.1 nm. Arrows indicate the three equivalent ⟨110⟩ directions in the (111) plane. Tunneling current 0.70 nA, bias voltage 0.9 V in both images.

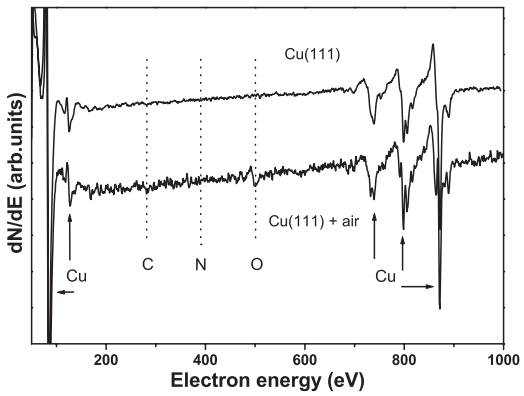

FIG. 2. Auger spectra of the Cu(111) surface before and after pulse injection of air, resulting in one monolayer coverage when the substrate was kept at ∼200 °C.

organic solvents used for cleaning the valve are driven into the deposition chamber because the valve was thoroughly cleaned with organic solvents and blown dry with nitrogen.

The peak-to-peak height ratio h_O/h_{Cu} is 0.048 for the lowest coverage obtained, where h_{Cu} is the peak-to-peak height at $E = 880$ eV. In the following, we will use the Auger ratio h_O/h_{Cu} as a measure of oxygen coverage. At the highest coverage (corresponding to one monolayer), the value of h_O/h_{Cu} is 0.145 and for the carbon peak we found $h_C/h_{Cu} = 0.036$. The value 0.145 is smaller than the saturation value $h'_O/h'_{Cu} \sim$ 0.22–0.23 reported for long-time exposures of UHV-cleaned Cu(111) to O_2 at $p_{O_2} = 1 \times 10^{-6}$ mbar.[17] In our case, the lower h_O/h_{Cu} ratio can be explained by the presence of carbon in the monolayer due to CO_2 or other carbon-containing impurities on the surface. Other works report a h_O/h_{Cu} ratio of ∼0.15 at RT,[6] at 220 °C,[23] and at 330 °C,[24] which is much closer to our measured value. CO_2 does not usually react with clean crystalline copper. A catalyst (e.g., alkaline atoms) is needed in order to activate its reaction.[25,26] Therefore, we expect the surface covered with oxygen coadsorbed with a small amount of carbon impurities or CO_2 molecules.

It is difficult to discriminate whether the AES oxygen peak originates from H_2O or from O_2 adsorbed on the surface since hydrogen can not be detected by AES. The sticking coefficient of O_2 on Cu(111) is reported to be low: $\sim 10^{-3}$ at RT and $\sim 3 \times 10^{-3}$ at 200 °C.[27] After deposition, O_2 molecules dissociate and are atomically adsorbed on Cu(111) at RT and higher temperatures.[5,8,17] The adsorption of H_2O on Cu(111) crucially depends on pressure, temperature, and surface cleanliness.[28] Furthermore, the amount of water vapor in air at RT (∼2 vol%) is much lower than the amount of oxygen (∼21 vol%). Similar to O_2, water is expected to dissociate into H and OH. Although coadsorption with oxygen can favor a further dissociation of the hydroxyl groups, it is not clear whether this does occur.[29] Rao *et al.*[30] reported different features in the oxygen KLL Auger line due to adsorbed water, atomic oxygen, or oxygen gas on Ag. These features are difficult to distinguish in our spectra because of the smallness of the oxygen signal.

The position of the nitrogen Auger peak at $E = 389$ eV is marked in the spectrum (Fig. 2). No indication of nitrogen is found, even though the Auger sensitivity factors of the Auger transition for N and O are very similar (1.2184 and 1.257,

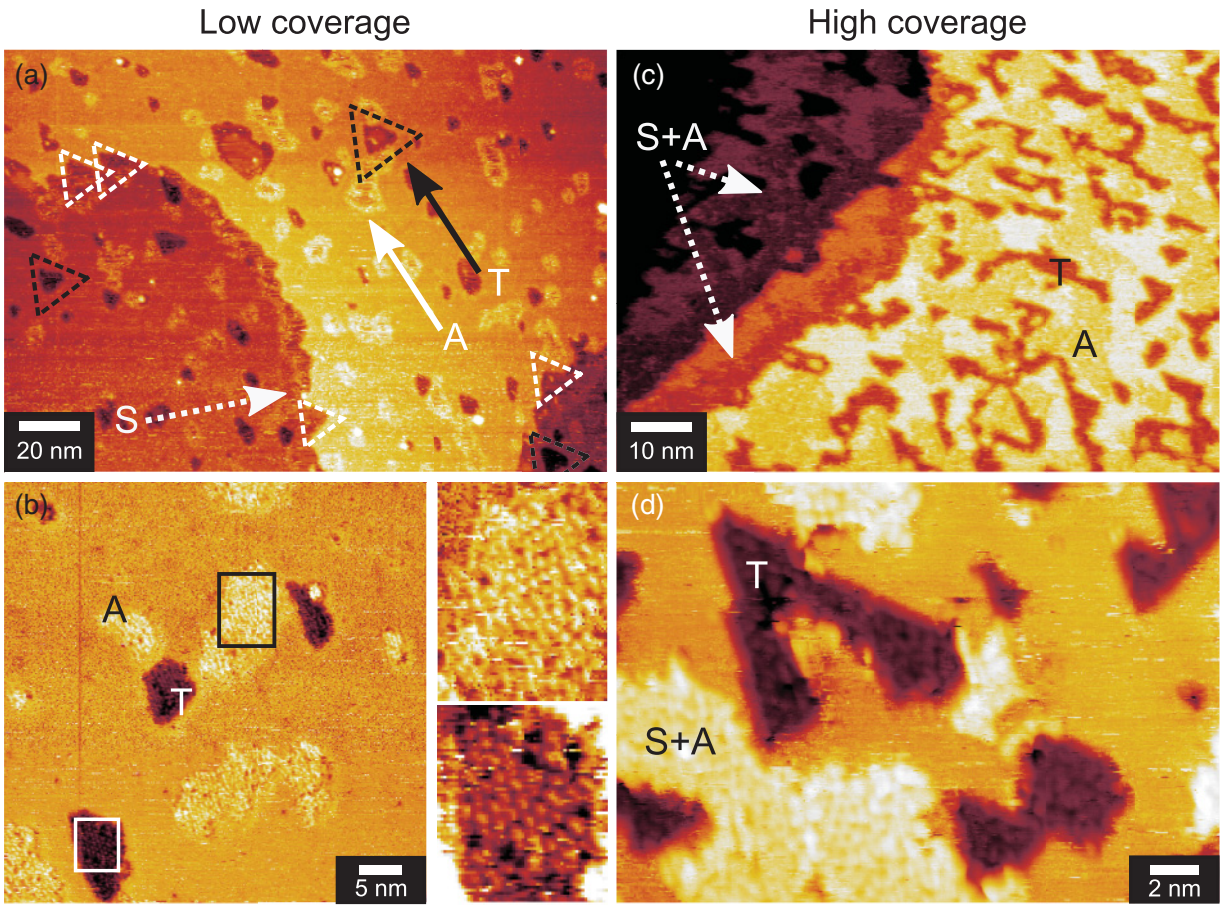

FIG. 3. (Color online) STM images of Cu(111) after exposure to air at RT: (a), (b) at low coverage and (c), (d) at high coverage. Dashed arrow and white triangles indicate angular step edges, solid white arrow indicates a bright island (A). Black arrow and triangles indicate dark islands (T). Low coverage: (a) image size 200 × 140 nm^2; tunneling current 0.20 nA and bias voltage 2 V. (b) 50 × 50 nm^2; 0.20 nA; 2 V. The magnified images of the marked regions reveal the internal structure of the A island (above), 7 × 9 nm^2, and the T island (below), 5.5 × 6.5 nm^2. High coverage: (c) 100 × 70 nm^2; 0.20 nA; 2 V. (d) Internal structures of T and S + A islands: 25 × 17.5 nm^2; 0.50 nA; 0.9 V.

respectively).[31] It has been reported that N does not chemisorb on copper directly unless the adsorption is activated by ion implantation or atomic beam sources.[32,33]

Regarding the possibility of hydrogen coadsorption, it is known that H_2 is absorbed at high pressure but desorbs again upon pumping, probably owing to its very small sticking probability.[34] In general, molecular H_2 is only adsorbed if activated by molecular collisions. We estimate the energy that the H_2 molecules can acquire by deposition with the pulse valve using the Bernoulli equation, with $\Delta p = 1$ bar. We obtain that air molecules (e.g., O_2 and N_2) will have an average velocity ∼390 m/s and a kinetic energy of ∼24 meV, whereas H_2 molecules will have ∼1490 m/s. However, due to the small amount of H_2 in ambient atmosphere, we expect that they will have a similar velocity to that of air molecules dominating the gas mixture while entering the chamber, which means a much lower energy of ≈1.5 meV. This is not large enough compared to the activation energy of 0.2 eV (Ref. 35) needed for adsorption on Cu.

C. Surface structures produced at room temperature

Figures 3(a) and 3(b) show STM images of the Cu(111) surface after exposure to air at RT with $h_O/h_{Cu} = 0.048$. The morphology of the copper surface is strongly affected by the exposure. The step edges are not smooth but rather angular, often with a triangular shape, some of which are marked with white dashed triangles [Fig. 3(a)]. These changes are accompanied by the appearance of fringes on the lower terrace close to the step edge, the contrast and apparent height of which strongly depend on the tunneling parameters. The fringes are labeled S and are indicated by the dashed white arrow in Fig. 3(a). In addition to these surface modifications close to the step edge, bright and dark islands appear on the terraces. The bright islands (labeled A, solid white arrow) show a contrast similar to that of the fringes at step edges, whereas the darker ones (labeled T, black arrow) show an apparent depth of approximately one atomic step.

In Fig. 3(b), the internal structure of the dark and bright islands is resolved. They appear to be composed of atomic-size protrusions with a nearest-neighbor distance of 0.55–0.65 nm. No long-range structural order is observed, only domains with a disordered hexagonal structure are seen. The internal order seems to be slightly higher in the T than in the A islands.

Figures 3(c) and 3(d) show STM images of the Cu(111) surface after exposure to air at RT at high coverage $h_O/h_{Cu} = 0.091$, but still well below one monolayer. Again, step

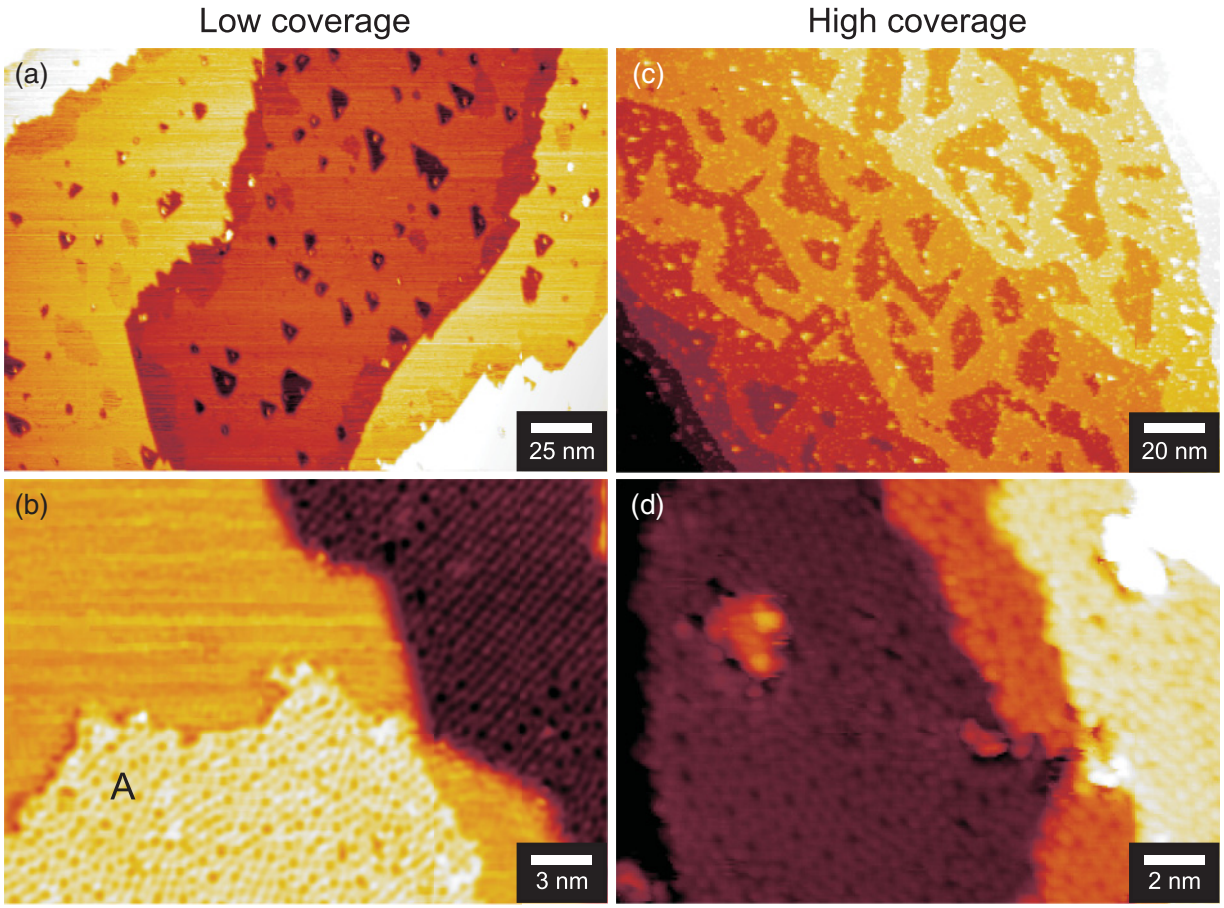

FIG. 4. (Color online) STM images of Cu(111) after exposure to air at $T \sim 200\,^{\circ}$C: (a), (b) at low coverage and (c), (d) at high coverage (one monolayer). Low coverage: (a) image size 250×175 nm^2; tunneling current 0.70 nA and bias voltage -36 mV. (b) Internal structure of T and A islands: 30×21 nm^2; 0.70 nA; 180 mV. High coverage: (c) 200×140 nm^2; 0.20 nA; 2 V. (d) Internal structure of T and S + A islands: 20×14 nm^2; 0.50 nA; 0.9 V.

edges are not smooth and appear to be accompanied by different islands. However, such structures exhibit differences in comparison with the features observed for low coverage [cf. Figs. 3(a) and 3(b)]. First, the step edges are not angular, but appear to be rather irregularly shaped [see Fig. 3(c)]. In addition, the three kinds of oxide (S, A, T) observed at low coverage are reduced to two, since S and A appear mixed together, especially in regions close to step edges. We denote them as A or S + A. Figure 3(d) displays the internal structure of T and S + A islands. As in the case of low coverage, regions with a more or less hexagonal lattice are present, but no long-range order is observed. The T islands (dark) display regular or polygonal borders of several adjacent triangles, whereas the shape of the A and S + A islands is rather irregular.

It is worth noting that some islands of T on the upper terrace transform into S across the step edge and are connected to A on the lower terrace without any separation or boundary between them. This indicates that the different islands (T, S, or A), have the same composition despite their different apparent contrast, shape, and internal ordering.

D. Surface structures produced at ∼200 °C

Figures 4(a) and 4(b) show STM images of the Cu(111) surface after exposure to air at higher temperature $T \sim 200\,^{\circ}$C at low coverage ($h_O/h_{Cu} = 0.046$). Similar to the deposition at RT, the surface is modified by the exposure to air and, aside from the fringes of the step edges (S), T and A structures are observed on the terraces. The shape of the dark islands seems to be more regular than those produced at RT. Figure 4(b) shows a smaller surface area with large T and A islands where the contrast has been adjusted to unveil their internal structure. Similar patterns show up in all kind of islands, however, the T and S ones (S not shown) display larger highly ordered domains.

Figures 4(c) and 4(d) show STM images of the Cu(111) surface after exposure to air at $T \sim 200\,^{\circ}$C at high coverage $h_O/h_{Cu} = 0.145$, corresponding to a coverage of one monolayer. Only bright and dark islands are observed on the surface. The change of morphology with increasing coverage was already reported in Sec. III C for exposures at RT, where the three different kinds of structures (T, A, S) observed at low coverage were reduced to two (T, S + A). The internal order of both islands is similar [see Fig. 4(d)], in contrast to images obtained at lower coverage [cf. Fig. 4(b)], where the internal order of the T islands appears to be higher. Hexagonally ordered patterns similar to those obtained at low coverage are observed. As already observed for RT deposition, T islands and S + A islands of low terraces intermix, pointing to the similarity of the two kinds of structures. In this case, both kinds of islands share the same border and display a similar shape.

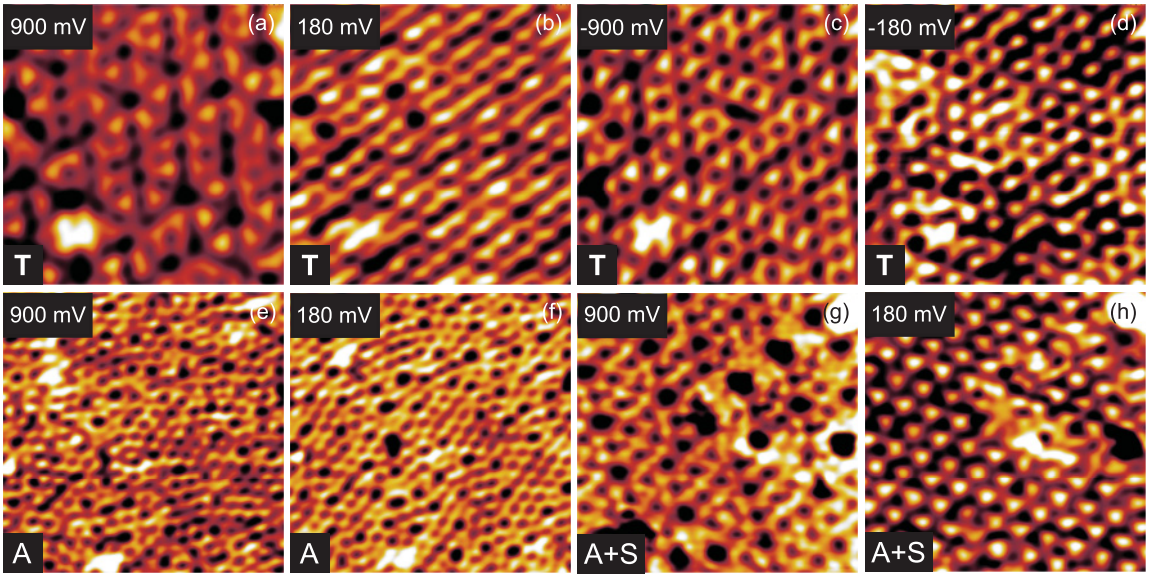

FIG. 5. (Color online) STM constant-current images at different voltages showing the internal structure of the (a)–(d) T island and (e), (f) A island of Fig. 4(b) at low coverage; and (g), (h) S + A at high coverage, all of them produced at $T \sim 200\,^{\circ}$C. Size of images (a)–(d) and (g), (h) 6×6 nm^2; images (e), (f) 10×10 nm^2; tunneling current (a)–(f) 0.7 nA and (g), (h) 0.5 nA.

The internal structure of the islands depends strongly on the tunneling parameters. In particular, the highly ordered domains with the hexagonal symmetry of the Cu(111) plane that appear on T and S islands at low coverage, and on T and S + A at high coverage, display different atomic-scale arrangements depending on the bias voltage. Figure 5 shows highly resolved constant-current STM images of different islands [Figs. 5(a)–5(f)] of hexagonal domains of T and A at low coverages, and an ordered S + A domain obtained at high coverage [Figs. 5(g) and 5(h)]. The structure of the ordered domains at low and high coverages appears to be similar.

IV. DISCUSSION

After pulse injection of air on the copper surface, mainly oxygen interacts with the surface, as inferred from AES. The effects and structures that we observe in our STM measurements have been already reported and described as Cu oxide or Cu oxide precursors formed by the reaction of oxygen with the Cu surface.[14,17] Oxygen is known from UHV experiments to adsorb dissociatively on Cu(111) above 170 K.[5,8,17] This adsorption takes place in or below the outermost plane of copper atoms,[5,7,10,14,17] and leads to the formation of surface oxide structures by incorporation of Cu atoms from step edges and terraces. The oxide islands nucleate at defect sites and step edges and grow by island formation.[5,14,17,36] These surface reactions are confirmed in our STM images.

Matsumoto *et al.* distinguished three different kinds of oxides at low coverage[14] (see schematic in Fig. 6):

(i) Fringes at step edges, denoted as "step oxide" (S). The injected air (mainly the oxygen) reacts with the Cu atoms at the step of the upper terrace, the latter are incorporated into the oxide islands growing on the lower terrace. As a result, the step edge of the upper terrace has an angular shape, and fringes of S appear on the lower terrace. The angular borders of the step edges prefer the orientation of the (111) symmetry directions of the surface [see Figs. 3(a) and 4(a)], as already reported.[14,17]

(ii) Dark oxide islands on the terraces, denoted as "terrace oxide" (T). The air reacts with the copper atoms that are at the edge of the vacancy islands or at atomic surface defects, which are incorporated into the oxide islands growing on the lower terrace. Hence, the oxide has a lower height than the unaffected part of the Cu terrace, which gives rise to a very dark contrast. T islands have a somewhat triangular form, the edges of which are parallel to the symmetry directions of the Cu(111) plane.

(iii) Bright islands on the terraces, denoted as "added oxide" (A). This oxide results from the reaction of oxygen with excess copper atoms liberated by the formation of T, and grows on the top of the terrace. Its different formation process leads to irregularly shaped islands.

Figure 7(a) shows an STM image of Cu(111) after exposure to air at $T \sim 200\,^{\circ}$C with several S, T, and A oxide islands. Figure 7(b) displays the height profile along the line drawn in Fig. 7(a). In that image, the oxide islands appear $\approx$0.075 nm lower than the oxygen-free parts of the terrace where they grow, thus, the dark T islands display a depth of one monoatomic Cu(111) step (0.208 nm) plus 0.075 nm

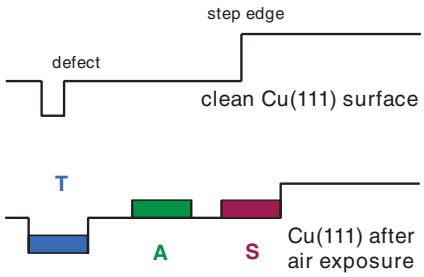

FIG. 6. (Color online) Schematic of the restructuring of the copper surface at initial stages of oxidation.

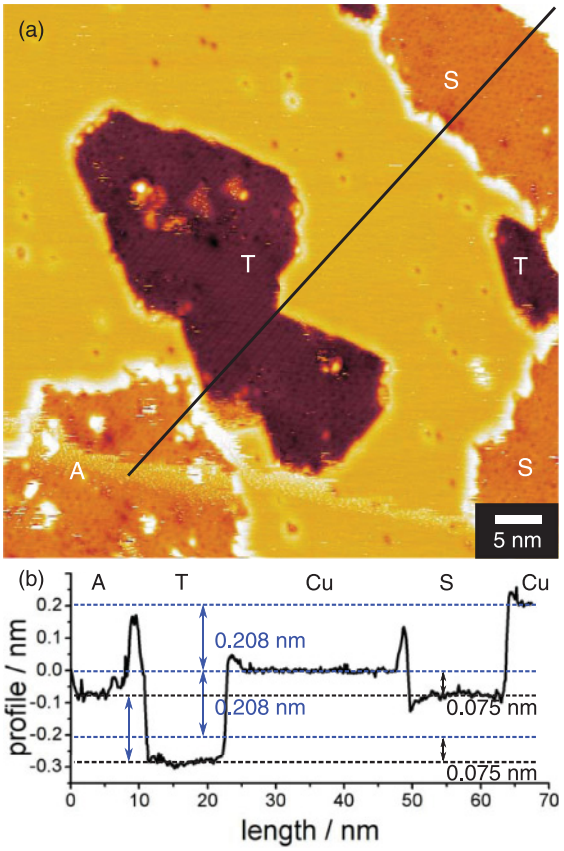

FIG. 7. (Color online) (a) STM image of Cu(111) after exposure to air at $T \sim 200\,^{\circ}$C. Image size 60×60 nm^2; tunneling current 0.70 nA; and bias voltage 0.9 V. (b) Height profile along the solid line in (a).

corresponding to the depth of the oxide layer. Their apparent height depends on the tunneling parameters due to the energy dependence of the local electronic density of states. As a consequence, the height that we measure does not correspond to the absolute height of the oxide structure, i.e., A islands in Figs. 3(d) and 4(b) appear to be on top of the terrace with a height of 0.10–0.15 nm, whereas in Figs. 3(c), 4(a), and 7(a), they appear to be lower than the terrace with a depth of 0.05–0.10 nm. The A and T islands of Fig. 4(b) correspond to the A and T islands of Fig. 7(a). This contrast leads to confusion since, although the growth takes place practically on top of the terrace as described in Fig. 6, in general the surface oxide structures display a darker contrast (i.e., lower conductance) than the clean Cu surface.

At high coverages, the three types of oxide structures are reduced to two, dark T and bright S + A islands, for both RT and 200 °C air injection. The shape of the T islands is the result of the coalescence of many triangular forms displaying a more regular shape than the bright islands (S + A). However, at one monolayer coverage, the islands are in close contact and their borders merge, i.e., some islands share the same border, thus resulting in a less polygonal/regular structure than at lower coverage. Figures 3(c) and 4(c) show that at high coverage, the different oxide islands are intermixed, in particular in the region where the step edges of the clean copper surface were originally located, suggesting that they have the same composition. Nevertheless, the oxide island shapes and their internal order differ in detail, depending on the temperature of the copper substrate during the exposure facilitating different nucleation processes.

Surface oxide structures produced at room temperature do not display long-range ordered domains, but only small regions with a loosely hexagonal ordering. The oxide islands are composed of small units that appear as protrusions in the STM images. These protrusions will be considered as molecular units of copper oxide.[14] They display a lateral nearest-neighbor distance of ∼0.55–0.65 nm and a corrugation of ∼0.05–0.1 nm. These structures are attributed to a disordered oxide precursor of Cu_2O,[2,10,14,15,17] with a lateral distance of 0.603 nm between oxygen atoms in the (111) plane. Several groups[6,8,10] have suggested that the copper surface reconstructs when oxidized at RT. The oxygen is expected to chemisorb on threefold hollow adsorption sites and partially penetrates into the surface layer, causing an increase of the in-plane Cu-Cu distance, which becomes similar to the Cu-Cu distance of $Cu_2O(111)$ epitaxially grown on Cu(111).[2,8] A similar behavior was reported for copper oxidation in aqueous solution[13] for which the reconstruction is produced by the adsorption of OH groups. This process possibly explains our STM images.

For exposures at $T \sim 200\,^{\circ}$C, large regions with highly ordered domains appear on the T and S islands, and at high coverage also on S + A islands. The lateral distance between nearest-neighbor oxide units is ∼0.6–0.61 nm and the corrugation ∼0.03–0.08 nm. The images of the internal structure of the oxide islands (arrangement and corrugation) strongly depend on the applied voltage. This is attributed to the fact that on metal-oxide surfaces, electronic states are generally more localized than on pure-metal surfaces, resulting in distinct maxima in the local density of states (LDOS) that give rise to a strongly voltage-dependent image contrast.[37] This renders the identification of atomic-scale patterns difficult, which therefore has to be based on the lattice constant and known symmetry of the imaged patterns.[37] Thus, we will compare our STM images with Cu_2O and Cu_2O-like patterns reported previously.

Several models have been proposed for the growth of surface oxide on the Cu(111) surface at high temperatures. In the following, we will focus on two of the most frequently reported patterns.

Model 1 [Fig. 8(a)]. Ho and Vook[4] investigated the initial overgrowth of cuprous oxide on Cu(111) at 350 °C by reflection high-energy electron diffraction (RHEED). They concluded that the overgrowth consists of a superlattice with a coincidence boundary at the $Cu_2O(111)$/Cu(111) interface. The oxide lattice is strained by the coincidence misfit of −1.22% with respect to the Cu(111) surface so that three times the overgrowth periodicity equals seven times that of the Cu substrate [6×7 coincidence site lattice (CSL)]. The resulting lateral distance between Cu_2O units is 0.595 nm. Such a commensurate structure has been also reported for Cu(111) oxidation investigated by x-ray diffraction studies in air (for very thin oxide films)[12] and in aqueous solution.[11,12] Recently, a high-resolution transmission-electron-microscopy (TEM) study of this misfit[18] suggested that the Cu_2O/Cu interface adopts a 5×6 CSL due to surface stress effects instead of a 6×7 CSL. The distance between Cu_2O units in this variant of model 1

(labeled 1′) is therefore 0.612 nm. Both models are compatible with the oxide lattices observed in our STM images, in particular, with images recorded at low bias voltage [see Figs. 8(b) and 8(c)]. The models do not specify the position of the copper and oxygen atoms relative to the copper surface; they only describe the periodicity of the Cu_2O units. Hence, we interpret the protrusions on the STM map as the oxide units grown on the Cu(111) surface. In our measurements, it was not possible to resolve the small difference of distance between nearest neighbors (0.595 and 0.612 nm) estimated for the two CSL, which renders a discrimination between models 1 and 1′ difficult.

Model 2 [Fig. 8(d)]. Two oxide precursor structures with very large cells called "29" and "44" have been reported for adsorption of O_2 on Cu(111) at high temperatures and/or subsequent annealing.[9,10,14,17] Such complicated patterns seem to correspond to a two-dimensional oxide layer with a distorted Cu_2O-like structure. Jensen *et al.*[9] presented a model for the oxygen-induced reconstruction of the Cu(111) surface, which resembles the (111) plane of the Cu_2O structure and consists

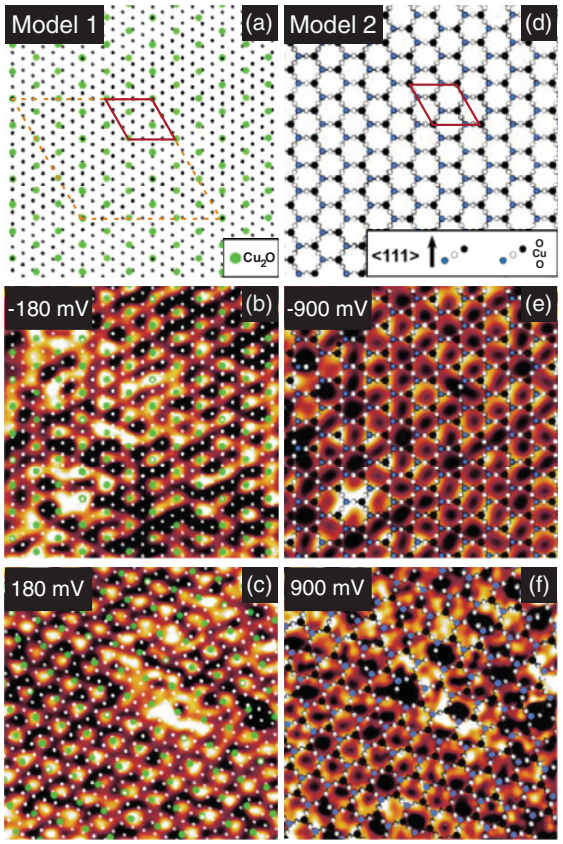

FIG. 8. (Color online) (a) Model 1 of the strained oxide lattice, after Ref. 4. Green circles indicate the periodicity of the Cu_2O lattice, black circles copper atoms. (b), (c) Superposition of the model on the STM images of T and S + A islands recorded at low bias voltage [(b) and (c) correspond to Figs. 5(d) and 5(h), respectively]. (d) Model 2: (111) projection of the first three planes of the Cu_2O-like model after Ref. 9. Black and blue circles indicate oxygen, white circles copper atoms. Inset shows a cross-sectional view of the first three planes. (e), (f) Superposition of the model on the STM images measured at higher bias voltage [(e) and (f) correspond to Figs. 5(c) and 5(g)]. Images size 6 × 6 nm^2. Surface unit cells are indicated by the solid and dashed lines.

of three oxygen planes coupled by copper planes. The (111) projection of the three first planes and a cross-sectional view (inset) are shown in Fig. 8(d). The outermost plane corresponds to oxygen atoms (black solid circles) laterally separated by 6.04 nm, forming a hexagonal lattice, followed by a copper plane underneath (white circles) with a distance between nearest neighbors of 3.02 nm, forming a honeycomb lattice, and further down oxygen (small blue circles) again separated by 6.04 nm and forming a hexagonal structure. This structure is labeled "model 2." The "29" and "44" superstructures correspond to the model of Jensen *et al.* with slightly distorted honeycombs. In our measurements, we do not observe such large cells characteristic for the distortion. They resemble, however, the nondistorted model as shown in Figs. 8(e) and 8(f), where model 2 is superimposed on the STM images. In this case, the model matches better the images measured at a larger bias voltage of ±0.9 V than images measured at lower voltages, e.g., Figs. 8(b) and 8(c) at ±180 mV. The dark patches appearing on the STM map are attributed to the holes in the $Cu_2O(111)$ surface. This model entails a considerable modification of the copper substrate, compared to model 1 since a trilayer structure is formed (each copper layer is sandwiched between two oxygen layers). A similar modification mechanism to the trilayer structure has been proposed by Lawson and Trapnell[38] for oxidation of Fe and Cu surfaces. Theoretical work[16] predicts that such a surface oxide is energetically very similar to the most stable case of a simple chemisorbed phase, indicating that the energy gained by forming such structure balances the energy needed to reconstruct the surface. Surface unit cells are shown in Figs. 8(a) and 8(d). The solid lines indicate equivalent unit cells for the models 1 and 2 with three Cu_2O units per cell. The dashed unit cell in Fig. 8(a) takes into account the overgrowth periodicity of the oxide on the Cu(111), including 27 Cu_2O units per cell.

Summarizing, the oxidation with air of the Cu(111) takes place by island formation. The ordering of the internal structure of the oxide islands increases with increasing coverage and copper exposure temperature, approaching that of the bulk Cu_2O oxide. The ordered domains produced at high temperature correspond to the strained Cu_2O lattice that coincides with the Cu(111) substrate as described by models 1, 1′, and 2, and also agree with theoretical results.[16] However, our results do not indicate the formation of large cells called "29" and "44" reported for adsorption of pure O_2 on Cu(111) at high temperatures and/or subsequent annealing[9,10,14,17] in the majority of STM studies of such oxidation process. We also investigated oxides prepared at higher exposures, giving rise to coverages above one monolayer (not shown). We found that these multilayers are difficult to measure with STM. However, sometimes atomic resolution was achieved and again structures of hexagonal symmetry were observed.

We now discuss briefly the effect of other molecules present in air but absent when exposing Cu(111) to pure O_2 or N_2 in UHV. Those may influence the adsorption and further dissociation of the reactive gas molecules (i.e., CO_2 and H_2O). On the one hand, this coadsorption may increase the temperature needed for the large cells of "29" and "44" structures. The subsequent annealing process desorbs the CO_2 and/or other carbon impurities that are probably coadsorbed with the oxygen and provides the energy the system needs for

producing such structures. On the other hand, the presence of hydroxyl groups from water coadsorbed with the oxygen may also play an important role on the arrangement of the adsorbates on the surface. However, due to dehydroxylation known to take place on Cu(111) above 200 K,[39] the amount of hydroxyl species is expected to be very small.

V. CONCLUSIONS

We have investigated the oxidation of Cu(111) by controlled air injection. We have shown that the nucleation of the oxide islands involves a restructuring of the copper surface, where Cu atoms from the step edges and terraces are incorporated into the growing surface oxide. At low coverage, three different oxide islands are formed (step, terrace, and added oxides), whereas at higher coverage, these are reduced to two (step-added and terrace oxides). These different kinds of oxide are formed by different processes, which lead to differences of the island shape and their internal ordering. However, we expect them to have the same composition since in some cases they appear mixed, without abrupt boundaries. Cu(111) oxide structures produced at RT are only poorly ordered. At $\sim$200 °C, highly ordered structures are observed. Atomically resolved images of the internal structure of the oxide islands strongly depend on the applied bias voltage. The lack of a detailed knowledge of the electronic structure renders the identification of atomic-scale patterns difficult because it has to be based solely on the lattice constant and known symmetry of the imaged patterns. The ordered structures correspond to a strained Cu_2O lattice that coincides with the Cu(111) substrate. The different experimental conditions systematically used in this work have a pronounced effect on the produced oxide patterns. Theoretical calculations are needed to disentangle the topographic and electronic contributions in the STM images.

ACKNOWLEDGMENTS

This work was supported by the Deutsche Forschungsgemeinschaft through the DFG Center for Functional Nanostructures (CFN) and the virtual Institute on Molecular Electronics supported by the Helmholtz Impuls- und Vernetzungs-Fond VH-FZ-021. The authors would like to thank D. Fujita and K. Sagisaka for permitting the performance of control experiments in their laboratory (NIMS), and M. Lukas and M. Marz for fruitful discussions.

*Present address: National Institute for Materials Science (NIMS), 1-2-1 Sengen, 305-0047 Tsukuba, Ibaraki, Japan; perezleon.carmen@nims.go.jp

[1] H. Tanaka and T. Kawai, J. Vac. Sci. Technol. B **15**, 602 (1997).
[2] G. Ertl, Surf. Sci. **6**, 208 (1967).
[3] G. W. Simmons, D. F. Mitchell, and K. R. Lawless, Surf. Sci. **8**, 130 (1976).
[4] J. H. Ho and R. W. Vook, J. Crystal Growth **44**, 561 (1978).
[5] L. H. Dubois, Surf. Sci. **119**, 399 (1982).
[6] H. Niehus, Surf. Sci. **130**, 41 (1983).
[7] R. W. Judd, P. Hollins, and J. Pritchard, Surf. Sci. **171**, 643 (1986).
[8] J. Haase and H.-J. Kuhr, Surf. Sci. **203**, L695 (1986).
[9] F. Jensen, F. Besenbacher, E. Lægsgaard, and I. Stensgaard, Surf. Sci. **259**, L774 (1991).
[10] F. Besenbacher and J. K. Nørskov, Prog. Surf. Sci. **44**, 5 (1993).
[11] N. Ikemiya, T. Kubo, and S. Hara, Surf. Sci. **323**, 81 (1995).
[12] Y. S. Chu, I. K. Robinson, and A. A. Gewirth, J. Chem. Phys. **110**, 5952 (1999).
[13] V. Maurice, H.-H. Strehblow, and P. Markus, Surf. Sci. **458**, 185 (2000).
[14] T. Matsumoto, R. A. Bennett, P. Stone, T. Yamada, K. Domen, and M. Bowker, Surf. Sci. **471**, 225 (2001).
[15] S. M. Johnson, A. Mulligan, V. Dhanak, and M. Kadodwala, Surf. Sci. **519**, 57 (2002).
[16] A. Soon, M. Todorova, B. Delley, and C. Stampfl, Phys. Rev. B **73**, 165424 (2006).
[17] F. Wiame, V. Maurice, and P. Markus, Surf. Sci. **601**, 1193 (2007).
[18] G. Zhou, Appl. Phys Lett. **94**, 233115 (2009).
[19] R. A. Evarestov and V. A. Veryazov, Phys. Status Solidi B **157**, 281 (1990).
[20] G. Honjo, J. Phys. Soc. Jpn. **4**, 330 (1949).
[21] A. Rönnquist and H. Fishmeister, J. Inst. Metals **89**, 65 (1960).
[22] C. Pérez León, C. Sürgers, M. Mayor, M. Marz, R. Hoffmann, and H. v. Löhneysen, J. Phys. Chem. C **113**, 14335 (2009).
[23] C. T. Campbell and K. A. Daube, J. Catal. **104**, 109 (1987).
[24] J. N. Russel, S. M. Gates, and J. T. Yates, Surf. Sci. **163**, 516 (1985).
[25] F. Solymosi, J. Mol. Catal. **65**, 337 (1991).
[26] S. Hadelfeldt, C. Benndorf, A. Stricker, and M. Töwe, Surf. Sci. **352**, 295 (1996).
[27] F. H. P. M. Habraken, E. Ph. Kiefer, and G. A. Bootsma, Surf. Sci. **83**, 45 (1979).
[28] A. Hodgson and S. Haq, Surf. Sci. Rep. **64**, 381 (2009), and references therein.
[29] M. A. Henderson, Surf. Sci. Rep. **46**, 1 (2002).
[30] C. N. R. Rao, M. W. Roberts, and P. Weightman, Philos. Trans. R. Soc., A **318**, 37 (1986).
[31] *Handbook of Auger Electron Spectroscopy*, edited by C. L. Hedberg, 3rd ed. (Physical Electronics, Eden Prairie, MN, 1995).
[32] J. F. Skelly, T. Bertrams, A. W. Munz, M. J. Murphy, and A. Hodgson, Surf. Sci. **415**, 48 (1998).
[33] D. Écija, J. M. Gallego, and R. Miranda, Surf. Sci. **603**, 2283 (2009).
[34] L. Österlund, P. B. Rasmussen, P. Thostrup, E. Lægsgaard, I. Stensgaard, and F. Besenbacher, Phys. Rev. Lett. **86**, 460 (2001).
[35] C. Engdahl, B. I. Lundqvist, U. Nielsen, and J. K. Nørskov, Phys. Rev. B **45**, 11362 (1992).
[36] N. Nilius, Surf. Sci. Rep. **64**, 595 (2009).
[37] T. Maroutian, S. Degen, C. Becker, K. Wandelt, and R. Berndt, Phys. Rev. B **68**, 155414 (2003).
[38] M. A. H. Lanyon and B. M. W. Trapnell, Proc. R. Soc. London, Ser. A **227**, 387 (1955).
[39] C.-T. Au, J. Breza, and M. W. Roberts, Chem. Phys. Lett. **66**, 340 (1979).